Eur. Phys. J. B **41**, 517–524 (2004)
DOI: 10.1140/epjb/e2004-00345-0

THE EUROPEAN PHYSICAL JOURNAL B

Amorphous to polycrystalline transition in Co_xSi_{1-x} alloy thin films

M. Vélez[1,a], C. Mény[2], S.M. Valvidares[1], J. Diaz[1], R. Morales[1], L.M. Alvarez-Prado[1], P. Panissod[2], and J.M. Alameda[1]

[1] Dpto. Física, Universidad de Oviedo, Av. Calvo Sotelo s/n, 33007 Oviedo, Spain
[2] IPCMS-GEMM (CNRS-UMR 7504) 23 Rue de Loess, 67037 Strasbourg Cedex, France

Received 7 April 2004 / Received in final form 26 July 2004
Published online 5 November 2004 –

Abstract. The transition from amorphous to polycrystalline microstructure has been studied in sputtered Co_xSi_{1-x} alloy films by structural, magneto-optical and Nuclear Magnetic Resonance measurements. For $x \geq 0.76$, Si is diluted into Co without significantly altering the polycrystalline microstructure, composed of a mixture of hcp and fcc grains. However, the fraction of Co atoms that contribute to the Nuclear Magnetic Resonance signal is found to decrease steeply (down to about 60% at $x = 0.76$) suggesting a microscopic segregation of a Si rich phase that induces a large degree of disorder. This is reflected in a harder magnetic behavior and a strong anisotropy dispersion. Below $x = 0.75$, the transition to an amorphous microstructure results in a sudden increase in the fraction of Co atoms within a ferromagnetic phase, indicating the recovery of the microscopic homogeneity. Also a significant enhancement of the macroscopic magnetic anisotropy is found for amorphous films with compositions right below the transition. Within the amorphous phase a second regime of Si segregation appears characterized by a constant Co local environment and constant magnetic properties. Finally, for $x = 0.65$ there is a significant Si enrichment in the Co environment and the films become non magnetic for compositions below this point.

PACS. 75.50.Kj Amorphous and quasicrystalline magnetic materials – 75.30.Gw Magnetic anisotropy – 76.60.-k Nuclear magnetic resonance and relaxation

1 Introduction

Magnetic metal – semiconductor systems have been the subject of intense experimental and theoretical work in recent years due to their relevance in the field of magnetoelectronics [1]. Among the simple binary TM-Si systems (TM = Fe, Ni, and Co) the first one, Fe-Si, has been the most extensively studied, both as Fe_xSi_{1-x} polycrystalline and amorphous alloys [2–6] and as Fe/Si multilayers [7–11]. In this last type of sample it has been shown that coupling effects between the magnetic layers are directly connected with the existence of Fe silicides at the interfaces, that can also affect their magnetoresistance properties [10].

In the Co-Si system, most of the interest has centered on the Si rich side of the phase diagram [12–15] where different crystalline phases $CoSi_2$, CoSi and Co_2Si have been identified. In particular, the good transport properties and high thermal stability of the $CoSi_2$ phase make it very suitable as a metal interconnect and gate contact in integrated devices [16–18]. Amorphous Co-Si alloys have received relatively less attention [19,20], even though they have a good potential for magnetooptical applications [21] and they appear widely in structural studies of different as-prepared and annealed Co-Si samples and Co/Si multilayers [22–25]. For example, crystalline silicides are often obtained via a solid state reaction from the annealing of an amorphous intermixed Co-Si layer [24]. In the case of Co/Si multilayers an oscillatory coupling has been predicted, related to the presence of quantum well states [26]. However, there exists conflicting experimental results on this issue [25,27] possibly due to the presence of amorphous Co-Si interfaces between the Co and Si layers that can strongly modify the structural and transport properties of the Co/Si multilayers [25].

In previous studies of Co-Si alloy films, such as the work by Fallon et al. [19], the presence of at least two different amorphous Co-Si phases have been reported depending on the Si concentration. However, the presence of microscopic compositional inhomogeneities in the films have made it difficult to correlate the structural characterization with the magnetic properties of the different magnetic phases observed. In this situation, a local probe is needed in order to obtain information not only on the average magnetic behavior of the sample but also on the magnetic environment of each Co atom.

In this work, we have performed an extensive structural and magnetic characterization of Co_xSi_{1-x} alloy thin films in the Co rich side of the phase diagram

[a] e-mail: mvelez@condmat.uniovi.es

($1 > x > 0.65$), focusing on the transition point from polycrystalline to amorphous microstructure that occurs at $x = 0.75$. Magnetooptical measurements have been combined with the local information provided by Nuclear Magnetic Resonance (NMR) studies in order to gain further insight into the processes that drive these microstructural changes in the Co-Si system and their influence on the magnetism of Co atoms.

2 Experimental

Co_xSi_{1-x} alloy films have been grown by dc magnetron sputtering on oxidized Si(111) substrates. The system base pressure is 10^{-8} mbar and the Ar working pressure during deposition is 10^{-3} mbar. 50 nm thick alloy films have been prepared by cosputtering from two independent pure Co and pure Si targets, and the composition varied from $x = 1$ to $x = 0.65$ by adjusting the relative power of the sputtering guns. The final alloy composition of each film was determined with an accuracy $\Delta x = \pm 0.01$ by electron probe X-ray microanalysis on a separate test sample grown simultaneously on a Cu substrate. Two series of samples have been grown, with deposition rates of 0.09 nm/s and 0.15 nm/s respectively, calibrated with a quartz microbalance, but the influence of this growth parameter was found to be negligible on the structural and magnetic properties of the films.

The films have been characterized by X-ray diffraction, Magnetooptical Transverse Kerr Effect (MOTKE) and Nuclear Magnetic Resonance (NMR). High angle $\theta - 2\theta$ X-ray diffraction patterns were measured in a Phillips diffractometer using Cu(Kα) radiation. MOTKE measurements were used to obtain the film's hysteresis loops from the change in reflectivity R induced by a magnetic field perpendicular to the incidence plane, as described elsewhere [28]. Transverse susceptibility measurements χ_t were also performed at 1 kHz, with a dc field of up to 400 Oe applied either along the hard or the easy axis in order to analyze the samples magnetic anisotropy [28,29]. All the magnetooptical measurements were taken at room temperature.

Zero field ^{59}Co Nuclear Magnetic Resonance (NMR) spectra were recorded at 1.5 K with an automated broadband NMR spectrometer. Beside the usual ω^2 correction of the spin echo intensity, the NMR intensity was also corrected for the enhancement factor. The enhancement factor was determined at each frequency from the dependence of the spin echo intensity upon the power excitation strength [30].

3 Results

3.1 Structural properties

The X-ray diffraction patterns of several Co_xSi_{1-x} alloy films have been plotted in Figure 1. Also indicated in this graph are the angular positions of the (100) and (002) peaks of bulk hcp Co ($2\theta = 41.78°$ and $44.82°$ respectively) with vertical dotted lines and that corresponding to the (111) peak of bulk fcc Co $2\theta = 44.36°$, marked with a vertical dashed line. For films with Co concentrations above $x = 0.76$ two well defined high angle peaks are present at $2\theta = 41.7°$ and $44.3°$, whereas in the diffraction patterns of the samples with $x = 0.75$ and 0.73 only a broad maximum centered about $2\theta = 44.5°$ can be observed. This change in the character of the diffraction pattern below $x = 0.76$ is similar to the behavior found in previous studies [19] and clearly marks a transition from polycrystalline to amorphous microstructure of the Co-Si alloy films as the Co content is reduced below this point. The angular positions of the peaks in the polycrystalline samples are consistent with a microstructure composed of a mixture of fcc and hcp phases, as is usually the case for pure polycrystalline Co thin films [31]. This indicates that the Si atoms are entering the Co lattice, forming a solid solution without significantly distorting the structure, similar to bulk Co-Si alloys in this composition range [32]. The grain size of the polycrystalline films, estimated from the width of the X-ray diffraction peaks using the Debye-Scherrer formula, is found to vary in the range 8 to 15 nm as the Si content is increased.

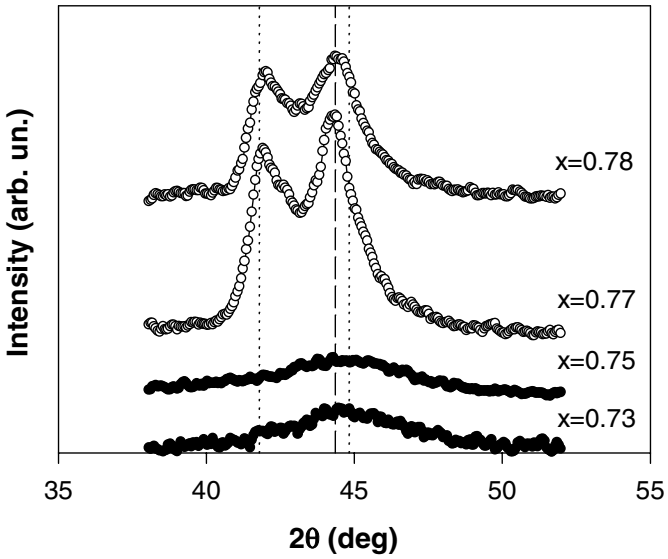

Fig. 1. X-ray diffraction patterns for several Co_xSi_{1-x} alloy films. The positions of the (100) and (002) peaks of bulk hcp Co are indicated by the vertical dotted lines while the position of the (111) peak of bulk fcc Co is indicated by a vertical dashed line. The X-ray patterns have been vertically displaced for clarity. Hollow symbols correspond to polycrystalline samples and filled symbols to amorphous ones.

3.2 Magnetic properties

A first insight into the effect of Si doping in the magnetic properties of these Co-Si samples can be obtained from the composition dependence of the magnetooptical parameter δ_K, shown in Figure 2. This is defined as

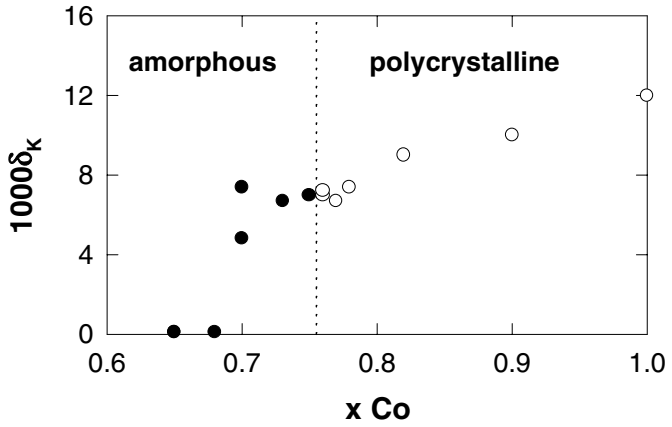

Fig. 2. Composition dependence of the magnetooptical parameter δ_K. Hollow symbols correspond to polycrystalline samples and filled symbols to amorphous ones. Dotted line indicates the amorphous to polycrystalline transition at $x = 0.76$.

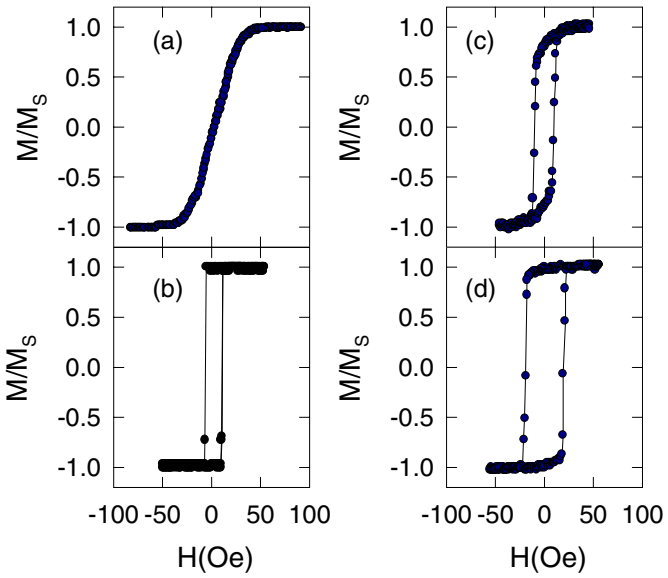

Fig. 3. In-plane hysteresis loops of two different Co_xSi_{1-x} samples: first, an amorphous $Co_{70}Si_{30}$ film with (a) H along the hard axis and (b) H along the easy axis and, second, a polycrystalline $Co_{76}Si_{24}$ film with (c) H along the hard axis and (d) H along the easy axis.

$\delta_K = (R_+ - R_-)/R$ where $R_+ - R_-$ is the total change in reflectivity caused by an inversion in sample magnetization and R is the reflectivity of an ideally demagnetized sample, usually obtained from the average value of R_+ and R_- [33]. In the case of films of thickness larger than the light penetration depth, as is the case here, and under similar measurement conditions, the evolution of δ_K in amorphous alloys of transition metal-metalloid [34] can be correlated to that of the material saturation magnetization, even though this parameter also contains information on the magnetooptical transitions related to the electronic structure of the medium [33].

The behavior that appears in Figure 2 shows a gradual decrease in the magnetooptical signal as the Co concentration decreases from $x = 1$ down to $x = 0.7$, that can be attributed to the progressive dilution of the Co atoms by the nonmagnetic Si atoms. However, no significant change in the magnetooptical response of the films is observed at the amorphous to polycrystalline transition (hollow symbols indicate polycrystalline samples and filled symbols correspond to amorphous ones). Finally, there is a sharp decrease in the δ_K values of the Co-Si samples for Co concentrations below $x = 0.68$, that indicates that in this composition range the samples are non magnetic at room temperature. This overall behavior is similar to that found for Fe-Si alloy films [34], only with a different composition range for the presence of amorphous magnetic samples, which can be related with the differences in the phase diagrams for bulk Fe-Si and Co-Si alloys [32].

The changes in the microstructure that occur at $x = 0.76$ are clearly reflected in the detailed magnetic behavior of the hysteresis loops, that can be seen in Figure 3 for an amorphous $Co_{70}Si_{30}$ film Figures 3a and b, and for a polycrystalline $Co_{76}Si_{24}$ film (i.e. with composition just above the transition), Figures 3c and d. The magnetic field is always applied in the sample plane, pointing either along the magnetic hard axis or along the magnetic easy axis, defined by the zero in the hysteresis loop of the perpendicular component of the magnetization [35].

All the magnetic Co_xSi_{1-x} films present an uniaxial behavior, but the anisotropy is much better defined for the amorphous samples: i.e. only in the composition range $0.7 \leq x \leq 0.75$, the hard axis hysteresis loops show a zero remanence (see Fig. 3a) and the easy axis loops are truly square with a reduced remanence M_r/M_S close to unity (see Fig. 3b). On the other hand, the polycrystalline films show rounded easy axis hysteresis loops and non zero coercivity for any angular position of the magnetic field. This reduced anisotropy in the behavior of the hysteresis loops of the polycrystalline films becomes more evident as the Co content decreases and the transition to amorphous microstructure is approached from above, as shown in Figures 3c and d.

It is also worth noting that the magnetic behavior is always harder for the polycrystalline films than for the amorphous ones. Figure 4a shows the composition dependence of the easy axis coercive field H_C for several films close to the amorphous to polycrystalline transition. The coercivity is almost constant for all the amorphous magnetic samples in the range $0.7 \leq x \leq 0.75$ with $H_C \approx 8$ Oe and, then, a sudden increase is observed when the samples become polycrystalline at $x = 0.76$ up to $H_C = 23$ Oe. Finally H_C decreases smoothly as the Co content is further increased, down to 7 Oe for the pure Co film. An interesting comparison can be made with the composition dependence of the anisotropy field H_K obtained from transverse susceptibility measurements. H_K values around 35 Oe are obtained for the amorphous magnetic samples with compositions far enough from the amorphous to polycrystalline transition. However, on the polycrystalline side of the graph, typical H_K values close to 25 Oe are found, i.e. $H_K \approx H_C$ for the polycrystalline Co-Si films

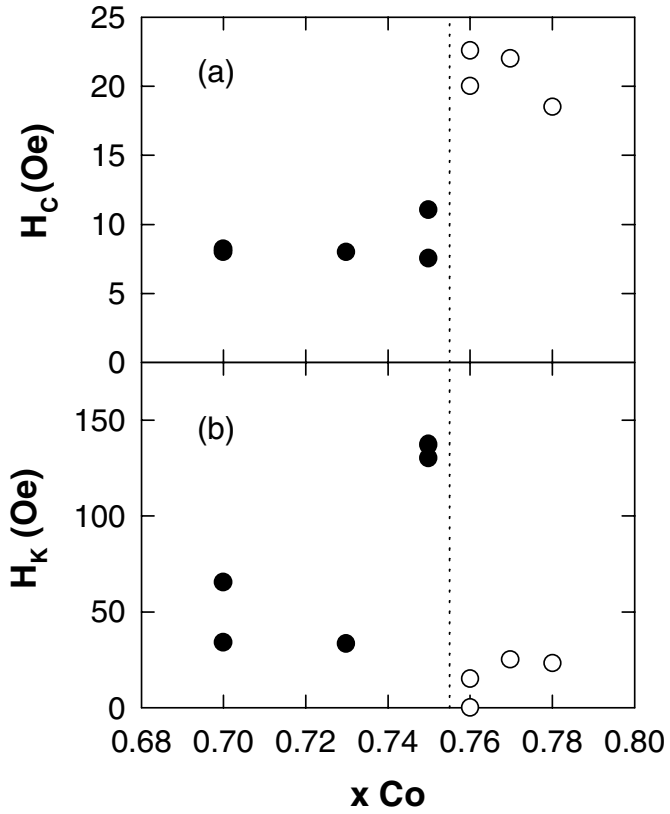

Fig. 4. (a) Composition dependence of (a) the easy axis coercive field and (b) the anisotropy field for Co_xSi_{1-x} films. Hollow symbols correspond to polycrystalline samples and filled symbols to amorphous ones. Dotted line indicates the amorphous to polycrystalline transition at $x = 0.76$.

indicating a reversal process controlled by the nucleation of inverted domains. The most important effects occur for compositions slightly above or slightly below the transition line. For $x = 0.75$ there are some very anisotropic films with H_K values up to 137 Oe, whereas the anisotropy is strongly suppressed for samples with $x = 0.76$ with an almost zero value of the anisotropy field.

3.3 NMR characterization

The results of the NMR characterization allow us to correlate these changes in the magnetic behavior of the Co-Si films at the amorphous to polycrystalline transition with the modifications taking place in the environment of the Co atoms (see Fig. 5 where the NMR spectra for a series of samples with decreasing Co content are plotted).

First of all, a detailed analysis of the pure Co sample gives fruitful information. Its NMR spectrum is characterized by a main contribution with a frequency close to 220 MHz. There is also an extended low frequency tail, typical of mixing at the Co/Si interface since the neighbourhood of Si atoms depresses the Co resonance frequency [36]. The main line frequency corresponds neither to bulk fcc Co (217 MHz) nor to bulk hcp Co (226 MHz). Indeed, even if the hyperfine field of bulk hcp Co is

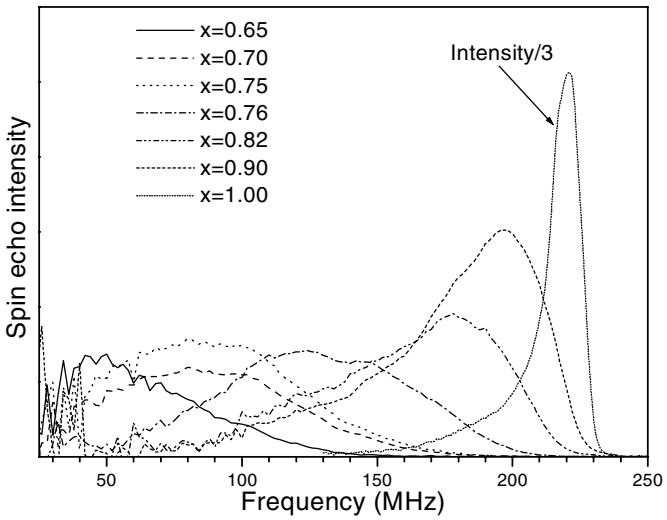

Fig. 5. NMR spectra of a series of Co_xSi_{1-x} alloy thin films, normalized to the samples surface area.

anisotropic, leading to two different resonance frequencies depending whether the magnetisation lies along the crystallographic c-axis (220 MHz) or perpendicularly to the c-axis (228 MHz), hcp polycrystalline samples would lead to an NMR spectrum showing a broad line with a main feature close to 226 MHz [37]. Therefore the observed 220 MHz resonance frequency has to be attributed to the presence of numerous stacking faults [38]. An additional shoulder close to 216 MHz can also be observed, showing the presence of a small amount of fcc Co. A simulation of the bulk part of this spectrum using the model of reference [39] shows that the main part of the Co atoms (about 75%) are in a hcp phase with a high concentration of stacking faults (40%). An estimate of the degree of intermixing at the Co/Si interface can be obtained from the intensity of the low frequency tail (<200 MHz) of the NMR spectrum. The amount of intermixed Co is of the order of 10 nm showing, as already reported in the literature, a high degree of intermixing.

This spectral response is gradually modified as Si doping is introduced into the films. The intensities of the NMR spectra plotted in Figure 5 are normalized to the samples surface area so that the integral intensity is proportional to the surface density of Co atoms that are within a ferromagnetic phase. Note that our NMR set up is dedicated to the analysis of ferromagnetic materials, therefore Co atoms that either do not carry a magnetic moment or that are within paramagnetic phases or superparamagnetic clusters will not contribute to the measured NMR signal [40]. Therefore, as expected with such a normalization, the total NMR intensity decreases with the decrease of the Co concentration and eventually, below a concentration of $x = 0.65$, the samples give no NMR signal indicating that they are no longer ferromagnetic.

From the behaviour of the spectra in Figure 5 three different regimes can be distinguished. The first one extends from $x = 1$, i.e. the pure Co sample, down to $x = 0.76$ and corresponds to the dilution of Si atoms into polycrystalline

Co. The spectra shift gradually towards lower frequencies since the neighborhood of Si atoms depresses the Co nuclei hyperfine fields and therefore depresses their resonance frequencies. The starting point of the second regime is the polycrystalline to amorphous phase transition that occurs between $x = 0.76$ and $x = 0.75$ and is characterized by an overall down frequency shift of the spectra. This second regime extends in the range $0.75 \leq x \leq 0.70$, corresponding to the first stage of Si dilution in the amorphous phase. Surprisingly the NMR spectra shapes do not change, meaning that the Co local environment stays unchanged with the increase of the Si content, and there is only a decrease in the total amount of Co atoms that contribute to the NMR signal Finally a significant Si enrichment of the Co neighborhood (the third regime) is shown by the NMR spectrum of the $Co_{65}Si_{35}$ sample. Below this concentration the samples lose their ferromagnetic character at 1.5 K.

4 Discussion

The changes in the NMR response upon Si doping can be characterized by the composition dependence of the spectra gravity center (see Fig. 6), which is proportional to the average magnetic moment carried by the Co atoms in ferromagnetic phases (i.e. by those that contribute to the NMR signal). This is different from bulk magnetometry measurements, in which the measured magnetic moment is usually normalized to the amount of deposited Co atoms; it therefore corresponds to the average moment over all the Co atoms present, independent of their environment. The position of the gravity center decreases smoothly upon increasing Si doping within the polycrystalline samples from 220 MHz down to 125 MHz at $x = 0.76$, until there is a sudden frequency down shift of about 25 MHz when the samples become amorphous at $x = 0.75$. Then, for the amorphous magnetic samples the average magnetic moment stays constant in the composition interval $0.75 \leq x \leq 0.70$, and, finally, it decreases again as the third regime is entered at $x = 0.65$.

The evolution in the fraction of Co atoms within ferromagnetic phases in each sample n_{Comagn}, given by the NMR intensity normalized by the total number of Co atoms, also shows a characteristic feature at the amorphous to polycrystalline transition (Fig. 7). Already below a concentration $x = 0.9$, a significant amount of the Co atoms are no longer in a ferromagnetic phase, and n_{Comagn} decreases below 60% as the polycrystalline to amorphous transition is approached from above. Then, as the samples become amorphous, there is a jump in the fraction of Co atoms that contribute to the NMR signal, up to almost 90% for $x = 0.75$. Finally, as the Si content increases within the amorphous phase, the fraction of Co atoms in a ferromagnetic phase decreases again, down to only 60% of the deposited Co atoms for the sample with the lowest Co content.

This fact suggests the existence of microscopic Si segregation between the different phases present in the polycrystalline films. This may be partly attributed to the

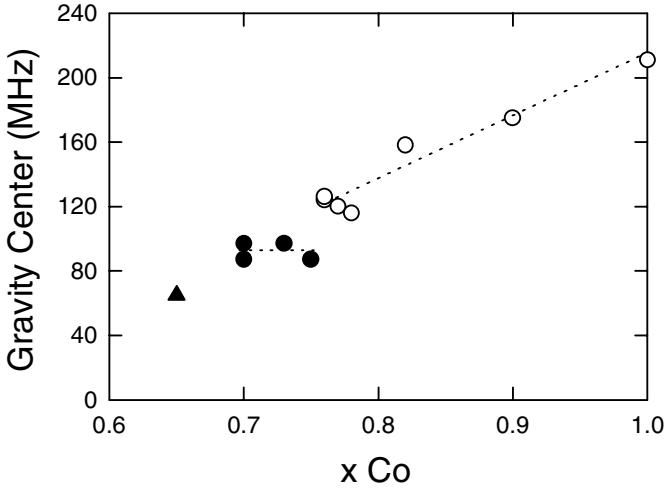

Fig. 6. Composition dependence of the position of the gravity center of the NMR spectra, related to the average magnetic moment per Co atom. Hollow circles correspond to polycrystalline samples, filled circles to amorphous films in the second regime of Si doping ($0.70 < x < 0.75$), and filled triangles to the amorphous films in the third regime ($0.68 > x$). Dotted lines are guides to the eye.

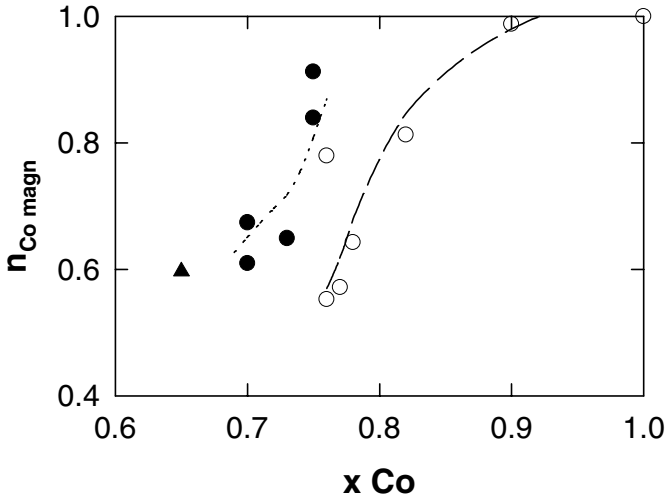

Fig. 7. Composition dependence of the fraction of Co atoms within a ferromagnetic phase n_{Comagn} within each film calculated from the NMR spectral intensity normalized by the number of Co atoms. Hollow circles correspond to polycrystalline samples, filled circles to amorphous films in the second regime of Si doping ($0.70 < x < 0.75$), and filled triangles to the amorphous films in the third regime ($0.68 > x$). Lines are guides to the eye.

different solubility of Si for fcc and hexagonal bulk Co-Si alloys: hexagonal phases (hcp Co solid solution and the metastable hexagonal Co_3Si phase) are present over a larger composition range in the Co-Si phase diagram than the fcc Co solid solution (stable only up to 16% Si) [32] so that there could be a mixture of Si-rich hcp grains with Si-poor fcc grains. Alternatively, this missing NMR intensity with the increase in Si content could also be explained by the presence of a small amount of other non magnetic

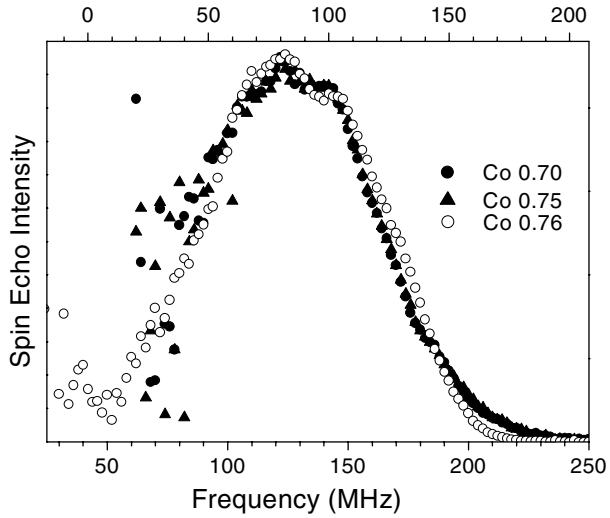

Fig. 8. Comparison of the NMR spectra shape for different Co_xSi_{1-x} films at both sides of the amorphous to polycrystalline transition, and within the amorphous magnetic phase. The spectra have been frequency shifted and normalized in order to allow for the direct comparison.

phases such as Co_2Si, which is possible according to the bulk phase diagram. One of the most intense peaks in the X-ray diffraction pattern of this phase is located at $2\theta = 44.14°$ which is quite close to those of fcc and hcp Co so that its presence in the samples cannot be ruled out from the X-ray data presented in Figure 1, even though no signature is found of any other reflections corresponding to it, which should appear at $2\theta = 44.1°, 45.3°, 46°$ or 48.6°. Notably, evidence was found in previous studies by Transmission Electron Microscopy [19] of the segregation of a lower density phase forming a structure of connected channels surrounding Co-rich regions both in the polycrystalline and amorphous regime of Co-Si alloy films.

As the polycrystalline to amorphous transition is approached at $x = 0.76$, the system pushes this microscopic Si segregation to its structural limit and the transition to the amorphous structure is marked by a recovery in the microscopic homogeneity, as indicated by the sudden increase in the fraction of Co atoms in a ferromagnetic phase up to almost 90%. It should be noted that the recovery in NMR intensity and the simultaneous down frequency shift at the polycrystalline to amorphous transition is not accompanied by any change in the shape of the NMR spectra. Indeed, as shown in Figure 8 the shape of the spectra for the amorphous sample ($x = 0.75$) is almost identical to the one of the polycrystalline sample ($x = 0.76$) once shifted to fit into the same frequency range. This shows that the local structure and short range order of the samples are identical on both sides of the polycrystalline to amorphous transition.

In the amorphous regime, further increasing the Si content ($0.7 < x < 0.75$) leads again to a decrease in the amount of Co atoms that contribute to the NMR signal, reflecting the presence of a second regime of phase segregation. In this regime the chemical composition of the ferromagnetic phase stays unchanged, as seen by the unchanged NMR response (Fig. 8). Only its total amount decreases as the Si content is increased. The increasing non (or very weakly) magnetic phase is most probably the one observed by NMR for a Co content of $x = 0.65$ and which has been analysed by EXAFS measurements as being an amorphous phase with a Co nearest neighbour environment close to disordered Co_2Si [41].

These changes in the local environment of the Co atoms observed by NMR provide a good understanding of the composition dependence of the magnetic properties of the Co-Si films, presented in the Results section. For example, the unchanged nature of the magnetic phase into the $0.7 < x < 0.75$ Co content regime is also observed in the magnetic properties of the samples. Indeed, in this regime the coercive fields as well as the anisotropy fields of the samples stay unchanged. Surprisingly below and very close to the amorphous transition a strong increase in the anisotropy field has been observed. The origin of this anisotropy field enhancement and the influence of the sputtering parameters is still under investigation.

In addition, some of the effects of the microscopic Si segregation suggested by the NMR data (which could include a reduced exchange coupling between magnetic grains) can be correlated with the magnetic behavior of the polycrystalline Co_xSi_{1-x} samples close to the transition: harder magnetic behavior and reduced anisotropy. Interestingly, in a narrow composition range close to $x = 0.76$ the films present an inverted magnetic behavior with H_K smaller than H_C, that is usually associated with a strong magnetization ripple caused by large random fluctuations in the local anisotropy direction at a microscopic level [42].

In general, the magnetic properties of both amorphous and polycrystalline films can be qualitatively understood in terms of a model of random local anisotropies [43]. These kinds of systems are characterized by the break up of the sample into small regions (coupling volumes) over which the local magnetization direction is correlated. The size of these regions, i.e. the magnetic correlation length L, is determined by the competition between the random local anisotropy and the exchange interactions, and can be calculated as a first approximation as [43]

$$L = 16A^2/9K_{loc}^2 d^3 \tag{1}$$

where K_{loc} is the magnitude of the local anisotropy, A is the exchange constant and d is the length scale for the spatial correlation of the magnetocrystalline anisotropy easy axes. In a polycrystal, d corresponds to the grain size, whereas in an amorphous sample d corresponds to interatomic distances (HPZ model [44]), at least in the limiting case of absence of any short range order. In this framework, the local anisotropy is averaged within each coupling volume, resulting in an effective anisotropy K_{eff} given by

$$K_{eff} = K_{loc}/N^{1/2} = K_{loc}/(L/d)^{3/2} \tag{2}$$

where N is the number of anisotropy distortions within each coupling volume. Thus, K_{eff} can be significantly

larger in polycrystalline films than in amorphous samples, simply due to the different d values, even if the local structure and short range order are very similar (as observed by NMR here). It must be noted that K_{eff} is again a random anisotropy term that is not directly related to the macroscopic anisotropy but, rather, when the magnetostatic energy is taken into account, it can be shown that the presence of K_{eff} results in the existence of a magnetization ripple in thin films. Notably, sufficiently strong induced anisotropy K_u is needed in order to give rise to ferromagnetic order ($K_u > K_{eff}$) [3,29], so that, in general, the macroscopic uniaxial anisotropy of the films will be better defined for small K_{eff} values (i.e. for small d and strong exchange interactions). In the framework of this random anisotropy model, the effects of microscopic segregation of a non-magnetic Si rich phase between Co-rich grains should manifest itself as a decrease in the exchange interactions between grains. This will lead to an enhanced K_{eff} and magnetization ripple which would explain the harder magnetic behavior and reduced macroscopic anisotropy observed in the hysteresis loops of the polycrystalline films with compositions just above the transition.

Transverse susceptibility measurements $\chi_t^{-1}(\beta)$, as shown in Figure 9 for several Co_xSi_{1-x} films with compositions close to the amorphous to polycrystalline transition, provide a good tool to analyze this behavior in detail. For the amorphous samples, Figure 9a, χ_t^{-1} presents a linear behavior down to $H = \pm H_K$ with a very small asymmetry in the position of the extrapolation to the abscissa for H along the easy axis ($\beta = 0°$) and H along the hard axis ($\beta = 90°$). This is typical behavior of real samples with a small magnetization ripple, i.e. $\chi_t^{-1}(\beta) \sim H \pm H_K + H_d$, where H_K is the macroscopic anisotropy field, related to K_u, H_d is the intrinsic demagnetization field, related to the shape of the coupling volumes,[29] and the positive sign corresponds to $\beta = 0°$ and the negative sign to $\beta = 90°$. From the obtained H_K values, the uniaxial anisotropy of the amorphous samples can be calculated as $K_u \approx 6 \times 10^3$ erg/cm^3, whereas a maximum value for $K_{eff} \approx 1$ erg/cm^3 can be estimated using $d = 0.25$ nm (HPZ model) and $K_{loc} \approx 10^7$ erg/cm^3 which is of the order of the maximum value of anisotropy constant observed for Co ($K = 6 \times 10^7$ erg/cm^3 in YCo_5 at 300 K [45]). Therefore, the condition $K_u > K_{eff}$ is easily fulfilled in the amorphous Co_xSi_{1-x} samples. It is worth noting that a similar behavior was also found in the $\chi_t^{-1}(\beta)$ vs. field curves of pure Co films [46], taking into account the contributions of both the fcc and hcp phases.

On the other hand, the polycrystalline Co_xSi_{1-x} films present a more isotropic behavior, indicated by the rounded character of the minima in the $\chi_t^{-1}(\beta)$ vs. field graphs (Figs. 9b and c), and the more pronounced asymmetry in the extrapolations to the abscissa, suggesting that in these samples K_{eff} and K_u are comparable. In particular, the behavior of the sample with $x = 0.76$, (Fig. 9b), in which the fraction of Co atoms in a ferromagnetic phase observed by NMR had been reduced below 60%, is characteristic of a sample composed of magnetically uncoupled regions with random anisotropy, in which the minimum in the $\chi_t^{-1}(\beta)$ vs. H curve corresponds to the anisotropy field of each region. Assuming a sample with a significant fraction of fcc Co (as is concluded from the analysis of the NMR and EXAFS [41] results) and a grain size of the order of 10 nm, L and K_{eff} can be estimated as $L = 70$ nm (much larger than d) and $K_{eff} = 2 \times 10^4$ erg/cm^3. The corresponding $H_{K_{eff}}$ value is of the order of 40 Oe, in good agreement with the position of the minimum in $\chi_t^{-1}(\beta)$ for this sample. Also, the observed coercive fields ($H_C \approx 20$ Oe) are about one half of this $H_{K_{eff}}$, as expected within the framework of Stoner-Wolfarth model for an ensemble of non-interacting uniaxial magnetic particles.

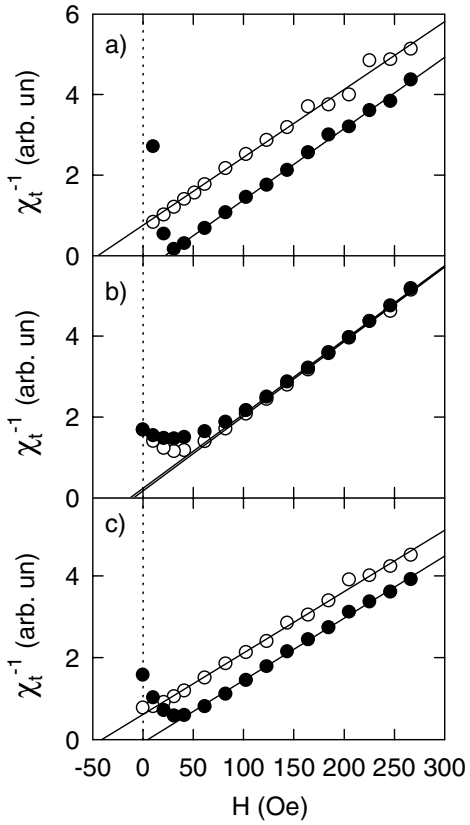

Fig. 9. Field dependence of the inverse transverse susceptibility $\chi_t^{-1}(\beta)$ for several Co_xSi_{1-x} films with H applied along the easy axis ($\beta = 0°$), hollow symbols, and with H applied along the hard axis ($\beta = 90°$), filled symbols: (a) $x = 0.73$; (b) $x = 0.76$; (c) $x = 0.77$. Solid lines are linear fits to the high field behavior. Note the asymmetry in the extrapolation to the abscissa in panels (b) and (c).

5 Conclusions

In summary, the changes in magnetic and structural properties of sputtered Co_xSi_{1-x} alloy films have been studied in the vicinity of the amorphous to polycrystalline transition. Starting from pure Co samples, a first regime of Si dilution into polycrystalline Co appears down to $x = 0.76$. It is marked by a microscopic Si segregation that results

in a steep decrease of the fraction of Co atoms within a ferromagnetic phase as the Si content increases, and in the occurrence of films with an inverted magnetic behavior ($H_C > H_K$) for $x = 0.76$ indicative of a sample composed of magnetically uncoupled regions with random anisotropy. As this microscopic Si segregation is pushed to its structural limit the polycrystalline to amorphous transition takes place for $x < 0.76$. This change to an amorphous microstructure is marked by the loss of high angle peaks in the X-ray diffraction patterns and a recovery in microscopic homogeneity indicated by the sudden increase in the fraction of Co atoms that contribute to the NMR signal and the well defined uniaxial magnetic anisotropy. Within the amorphous phase, the fraction of Co atoms in a ferromagnetic phase gradually decreases upon increasing Si content, keeping constant the average magnetic moment, indicating a second regime of phase segregation. Finally, a significant Si enrichment in the Co environment is found for $x = 0.65$, and the ferromagnetic character is lost for films beyond this composition point.

Work supported by Spanish CICYT under grant MAT2002-04543-C02-01 and HF/2002-0170.

References

1. G. Prinz, Science **282**, 1660 (1998)
2. Ph. Mangin, G. Marchal, J. Appl. Phys. **49**, 1709 (1978)
3. J.M. Alameda, C. Contreras, H. Rubio, Phys. Stat. Sol. (a) **85**, 511 (1984)
4. Y. Shimada, H. Kojima, J. Appl. Phys. **47**, 4156 (1976)
5. C.N. Afonso, A.R. Lagunas, F. Briones, S. Girón, J. Magn. Magn. Mater **15-18**, 833 (1980)
6. J.A. Aboaf, R.J. Kobliska, E. Klokholm, IEEE Trans. Magn. **14**, 941 (1978)
7. J.A. Carlisle, A. Chaiken, R.P. Michel, L.J. Terminello, J.J. Jia, T.A. Callcott, D.L. Edever, Phys. Rev. B **53**, 8824 (1996)
8. L.M. Alvarez-Prado, G.T. Perez, R. Morales, F.H. Salas, J.M. Alameda, Phys. Rev. B **56**, 3306 (1997)
9. G.J. Strijkers, J.T. Kohlhepp, H.J.M. Swagten, W.J.M. de Jonge, Phys. Rev. Lett. **84**, 1812 (2000)
10. H.C. Herper, P. Weinberger, L. Szunyogh, C. Sommers, Phys. Rev. B **66**, 064426 (2002)
11. J.M. Pruneda, R. Robles, S. Bouarab, J. Ferrer, A. Vega, Phys. Rev. B **65**, 024440 (2002)
12. A.E. White, K.T. Short, R.C. Dynes, J.P. Garno, J.M. Gibson, Appl. Phys. Lett. **50**, 95 (1987)
13. H. von Kanel, C. Schwarz, S. Goncalves-Conto, E. Muller, L. Miglio, F. Tavazza, G. Malegori, Phys. Rev. Lett. **74**, 1163 (1995)
14. G. Ottaviani, K.N. Tu, C. Nobili, J. Appl. Phys. **62**, 2290 (1987)
15. O. Ersen, V. Pierron-Bohnes, M.-H. Tuilier, C. Pirri, L. Khouchaf, M. Gailhanou, Phys. Rev. B **67**, 094116 (2003)
16. J.Y. Shin, S.W. Park, H.K. Baik, Thin Solid Films **292**, 31 (1997)
17. W.W. Wu, T.F. Chiang, S.L. Cheng, S.W. Lee, L.J. Chen, Y.H. Peng, H.H. Cheng, Appl. Phys. Lett. **81**, 820 (2002)
18. S.B. Herner, M. Mahajani, M. Konevecki, E. Kuang, S. Radigan, S.V. Dunton, Appl. Phys. Lett. **82**, 4163 (2003)
19. J.M. Fallon, C.A. Faunce, P.J. Grundy, J. Phys.: Condens. Matter **12**, 4075 (2000)
20. Y.Q. Liu, G. Shao, K.P. Homewood, J. Appl. Phys. **90**, 724 (2001)
21. J.H. Cai, W. Yang, T.J. Zhou, G. Gu, Y.W. Du, Appl. Phys. Lett. **74**, 85 (1999)
22. P. Ruterana, P. Houdy, P. Boher, J. Appl. Phys. **68**, 1033 (1990)
23. J.M. Fallon, C.A. Faunce, P.J. Grundy, J. Appl. Phys. **88**, 2400 (2000)
24. W. Lur, L.J. Chen, Appl. Phys. Lett. **54**, 1217 (1989)
25. P.J. Grundy, J.M. Fallon, H.J. Blythe, Phys. Rev. B **62**, 9566 (2000)
26. J. Enkovaara, A. Ayuela, R.M. Nieminen, Phys. Rev. B **62**, 16018 (2000)
27. K. Inomata, Y. Saito, J. Appl. Phys. **81**, 5344 (1997)
28. J.M. Alameda, F. Lopez, Phys. Stat. Sol. (a) **69**, 757 (1982)
29. H. Hoffmann, Phys. Stat. Sol. **33**, 175 (1969)
30. P. Panissod, J.P. Jay, C. Mény, M. Wojcik, E. Jedryka, Hyperfine Interact. **97-98**, 75 (1996)
31. G.J. van Gurp, J. Appl. Phys. **46**, 1922 (1975); J.L. Bubendorff, C. Mény, E. Beaurepaire, P. Panissod, J.P. Bucher, Eur. Phys. J. B **17**, 635 (2000)
32. K. Ishida, T. Nishizawa, in *Binary Alloy Phase Diagrams*, Vol. 2, edited by T.B. Massalski, H. Okamoto, P.R. Subramanian, L. Kacprzak (ASM International, 1996), p. 1235
33. A.K. Zvezdin, V.A. Kotov, *Modern Magnetooptics and Magnetooptical Materials* (Institute of Physics, Bristol, 1997)
34. J.M. Alameda, J.F. Fuertes, D. Givord, A. Liénard, B. Martínez, M.A. Moreu, J. Tejada, J. Phys. Colloq. France **49**, C8-1789 (1988)
35. M. Prutton, *Thin Ferromagnetic Films* (Butterworths, London, 1964), p. 103
36. P.C. Riedi, R.G. Scurlock, J. Appl. Phys. **39**, 1241 (1968)
37. H.A.M. de Gronckel, Ph.D. thesis, Eindhoven University of Technology, 1993
38. H.A.M. de Gronckel, P.J.H. Bloemen, E.A.M. van Alphen, W.J.M. de Jonge, Phys. Rev. B **49**, 11327 (1994)
39. A. Michel, V. Pierron-Bohnes, J.-P. Jay, P. Panissod, S. Lefebvre, M. Bessiere, H.E. Fischer, G. Van Tendeloo, Eur. Phys. J. B **19**, 225 (2001)
40. P. Panissod, in *Frontiers in Magnetism of Reduced Dimension Systems*, NATO ASI Series 49, edited by Bar'yakhtar, Wigen, Lesnik (Kluwer Academic, Dodrecht, 1998), p. 225
41. M. Velez, S.M. Valvidares, J. Diaz, R. Morales, J.M. Alameda, IEEE Trans. Magn. **38**, 3078 (2002)
42. H. Riedel, Phys. Stat. Sol. (a) **24**, 449 (1974); J.M. Alameda, M.C. Contreras, F. Carmona, F. Lopez, Phys. Stat. Sol. A **107**, 329 (1988)
43. R. Alben, J.J. Becker, M.C. Chi, J. Appl. Phys. **49**, 1653 (1978)
44. R. Harris, M. Plischke, M.J. Zuckermann, Phys. Rev. Lett. **31**, 160 (1973)
45. J.M. Alameda, D. Givord, R. Lemaire, Q. Lu, J. Appl. Phys. **52**, 2079 (1981)
46. J.M. Alameda, F. Lopez, Phys. Stat. Sol. (a) **69**, 757 (1982)